

Bridgeless single stage AC/DC converter with power factor correction

Anurag Sharma, Rajesh Gupta

Power Electronics Research Laboratory, Department of Electrical Engineering, Motilal Nehru National Institute of Technology Allahabad, Prayagraj, India

Article Info

Article history:

Received Jan 9, 2022

Revised May 9, 2022

Accepted Jul 11, 2022

Keywords:

AC-DC

Bridgeless

Isolated

PFC

Rectifier

ABSTRACT

This research paper proposes a novel bridgeless single-stage isolated converter with power factor correction and load voltage control. The proposed converter reduces the input diode bridge requirement with reduced passive components and provides a unidirectional flow of power to the load. The single-stage design reduces the use of an electrolytic capacitor, which improves reliability and reduces the size of the converter. The proposed control method is based on a single proportional integral (PI) controller to achieve both power factor correction and input current control. The proposed bridgeless converter is suitable for electric vehicle (EV) charging. A simulation study is performed on the MATLAB/Simulink to verify the effectiveness of the proposed converter. The converter is implemented in the laboratory to obtain the experimental results using typhoon hardware in the loop (HIL) based real time simulator.

This is an open access article under the [CC BY-SA](https://creativecommons.org/licenses/by-sa/4.0/) license.



Corresponding Author:

Anurag Sharma

Power Electronics Research Laboratory, Department of Electrical Engineering, Motilal Nehru National Institute of Technology Allahabad, Barrister Mullah Colony, MNNIT Allahabad Campus

Teliarganj, Prayagraj, Uttar Pradesh 211004, India

Email: anuragsharma@mnnit.ac.in

1. INTRODUCTION

Traditionally, the single-stage AC/DC converters are limited only to low-power applications such as the light emitting diode (LED) power supply. The major limitations faced by the single-phase single-stage (SPSS) isolated rectifiers are the reduced efficiency which limits the use of these converters for high power applications. However increased application of power electronics equipment such as different types of chargers for a variety of equipment, has opened up an area where the benefit of the SPSS converters such as reduced size, simpler architecture, and lower magnetic components have become significant.

Kushwaha and Singh [1] has shown implementations of the variations of the flyback converter-based electric vehicle (EV) chargers with isolation. These chargers were designed for the low-powered battery packs used in the E-rickshaws. A similar configuration of the EV chargers has been introduced which is the combination of the flyback converter with other DC to DC converters such as Cuk, single-ended primary-inductor converter (SEPIC) [2], LUO [3], and Landsman [4] converters. These proposed converters are used in the bridgeless configurations to reduce the losses associated with the forward resistance in the diode bridge in the power factor correction (PFC) rectifier. All of the above-listed converters are two-stage converters where the first stage is used to provide a PFC and the second stage is an isolation stage that performs the AC-DC conversion. All the discussed converters in [5]-[9] have the DC link capacitor. From [10]-[12], the SPSS converters discussed are limited to the low level of power. The novel converter in [13] has a low power level but provides a larger range of operating voltages. The circuit is derived from the

conventional PFC rectifier having a boost converter followed by a diode bridge rectifier. However, it has a simple circuit but it has many magnetic components which are difficult to design. Wu and Chen [14] an attempt is made to achieve more power in the SPSS converter but it leads to more number of switches.

The control method is based on the variable frequency control and is able to achieve the high-power factor and work in accordance to the IEC6100-3-2 class D standards. The power level up to 1.0 kW and 3.3 kW was achieved in the SPSS converter using an H-bridge-based converter [15]. The converter also uses extra switches connected in back-to-back configuration to achieve power factor correction function. Since the switch count in [16] was very high when compared to a single-phase application, an improvement was made by reducing the number of switches and maintaining the features of power factor correction and high-power levels. A modular three-phase configuration of delta isolated SEPIC converter [17] with sliding mode control was studied to accomplish the power factor correction with simultaneous charging of the EV battery. The proposed modular configuration in [17] uses three Cuk rectifier modules with their output connected together while using the sliding mode control for the PFC and EV charging. The dual-stage conversion has reduced efficiency hence single-stage conversion with PFC operation is an area of investigation. It introduced a single-stage AC/DC converter that has both vehicle-to-grid (V2G) and grid-to-vehicle (G2V) support. The bidirectional single-stage AC-DC converter [18] uses a large number of switches which can be reduced if a unidirectional approach is used. The converter from [19], [20] has reduced the number of switches but requires a diode bridge on the AC side which again contributes to higher losses. It uses the proportional-integral-derivative-based (PID-based) control algorithm to obtain the power factor correction and desired output voltage. Zhang *et al.* [21], for increasing the power level the three-phase single-stage converter is designed with the help of switch mode rectifier and high-frequency isolation. A single-stage converter with low number of components is discussed however the power levels are low and the total number of diodes used is also higher, which will contribute to more losses [22]. A novel EV charger in [23] with a reduced state of conversion is studied but the switching devices used in the converter were more, thus it was not a cost-effective solution. A reduced component converter for single stage operation is introduced in [24], [25], but the elimination of input diode bridge is neglected leading to the more use of diodes which discussed earlier contribute to the losses. A matrix converter-based single-stage converter is discussed which also suffers from the drawback of a large number of switches and also delivers powers that are not significantly higher when compared to the earlier discussed topologies [26], [27]. A comparison of the existing single-stage isolated converter is discussed in Table 1.

The proposed converter uses a novel single-stage AC-DC converter with isolation to reduce the need for an electrolytic capacitor by eliminating the intermediate DC-DC conversion stage and utilizing two medium-frequency transformers. This paper proposes a bridgeless single-stage isolated converter that can both achieve improved input power factor correction and load voltage control. The proposed converter reduces the input diode bridge requirement with reduced passive components and provides a unidirectional flow of power to the load in a single stage. It eliminates the requirement of the electrolytic capacitor, which improves reliability and reduces the size of the converter. The proposed converter consists of four MOSFET switches connected in back-to-back configuration which enables the controlled flow of the current. The control of the converter is based on the PI controller to achieve PFC operation and output voltage control. The simulation study of the proposed converter is done on the MATLAB/Simulink software and the experimental results are obtained through the typhoon hardware in the loop-based (HIL-based) real time simulator.

Table 1. Comparison of different SPSS converter topologies

Reference	Isolated	Switches	Output diodes	Power	Power flow
[15]	Yes	10	4	3 kW	Unidirectional
[16]	Yes	5	12	3 kW	Unidirectional
[17]	Yes	8	0	3 kW	Bidirectional
[18]	Yes	16	4	3 kW	Unidirectional
[19]	Yes	5	4	2 kW	Unidirectional
[20]	Yes	2	1	500 W	Unidirectional
[23]	Yes	10	0	3.3 Kw	Bidirectional
[26]	Yes	12	0	1,500 W	Bidirectional
Proposed converter	Yes	4	2	1 Kw	Unidirectional

2. CIRCUIT OPERATION AND CONTROL

Figure 1 shows the proposed single-stage isolated converter for EV charging application. The converter consists of four MOSFET switches, where the switch S1 and S2 are connected in back-to-back configuration to control the flow of current from point a to b and b to a, as per Figure 1. The diodes D1 and D2 are also connected back-to-back which prevents the shorting of the input from the input AC, in both the

positive and the negative half of the cycle. Transformer TX is a 1:n ratio high-frequency transformer with center tapping on both sides. The objective of the center tapping is to provide the path via diode D1 and D2 to the input, thus maintaining a constant flow of the current. The center tapping also reduces stress on the transformer winding by distributing the load between the two transformer windings. The output diodes D3 and D4 are conducting only one at a time thus the number of diodes in conduction mode is reduced which reduces the losses due to diode as in the case of PFC rectifier with an input diode bridge.

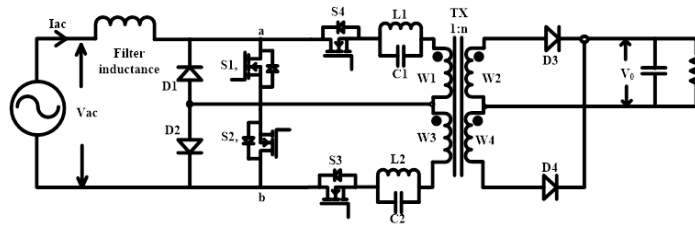


Figure 1. Proposed single-stage AC/DC converter

Figures 2(a) and 2(b) shows the conduction of switches in the positive cycle of the input AC current. During the positive half of the input voltage, the switch S4 is on. This charges the tank resonant circuit and during this period the magnetic energy is stored in the core of the transformer and is transferred to the load via diode D3. When S4 is on there is a fall in the ac current I_{ac} , which is then compensated by turning on the switch S1. The current now flows through the switch S1 and the feedback diode of S2, as seen in Figure 2(b). This forces the complete input voltage across the filter inductance and causes the rise of the current I_{ac} . During this period the stored magnetic energy is discharged through the diode D3. As per Figure 3(a) and 3(b), in the negative cycle, the operation is shifted from S1, S4 to S2, S3. In Figure 3(a) when the input voltage is in a negative half cycle, the switch S3 operates. This leads to the flow of current into the lower primary side winding W3 and passes through the diode D1. On the secondary side, the energy is transferred to the load via diode D4. During this period the input AC current rises as the load is connected via transformer winding W3. To reduce this current rise, the switch S2 is turned on leading to a reverse voltage polarity to be applied across the inductor thus reducing the current as shown in the Figure 3(b). During this period the stored energy in the core of the transformer is transferred to the load via diode D4 thus preventing the saturation of the core.

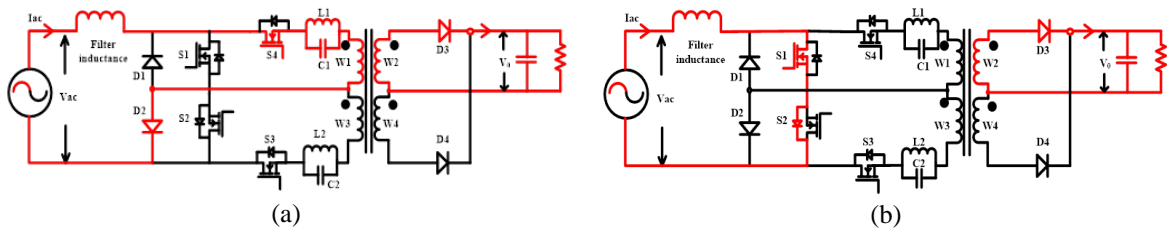


Figure 2. The circuit operation showing (a) flow of current in the circuit when S4 is in ON state and (b) flow of current in the circuit when S1 is in ON state

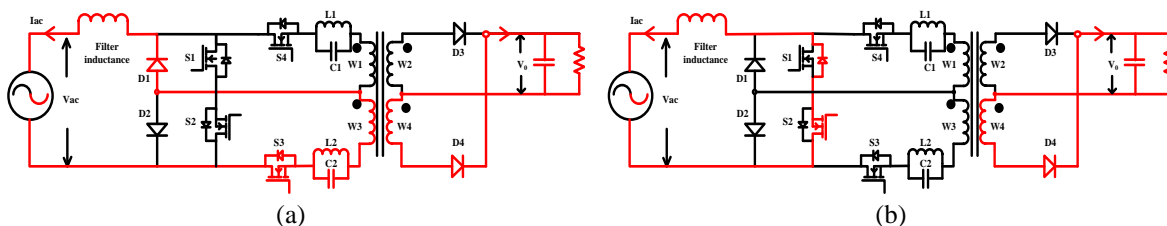


Figure 3. The circuit operation showing (a) flow of current in the circuit when S3 is in ON state and (b) flow of current in the circuit when S2 is in ON state

2.1. Control of the converter

The control of the proposed converter is shown in Figure 4. The control method implements the phase-locked loop and DC-link voltage control. The error between the DC-link voltage and the reference DC-link voltage is fed to a PI controller to produce a reference peak current I_R , which is then multiplied with a unit template sinusoid to produce a reference current I_{ref} . Since I_{ref} is in phase with the input voltage the error produced between I_{ref} and I_{ac} is compared to K to produce the control pulse. Thus K is directly controls the PFC and total harmonic distortion (THD). The theoretical waveform for the reference current and the load current is represented in Figure 5. The variation in the ac current is controlled by the constant K as discussed in Figure 4. This lets the ripple be maintained within I_{ref} and $I_{ref} + K$, when the current is in the rising phase that is the duration when the current moves from $I_{ref} + K$ to I_{ref} , switch $S1$ and $S3$ are on. Due to the proposed circuit configuration, the turning of switch $S3$ doesn't affect the flow of current and it will still pass-through switch $S1$ and feedback diode $S2$. Similarly, during the fall of the input AC current from I_{ref} to $I_{ref} + K$, the switch $S4$ will conduct and the same pulse can be given to $S2$ as it will not produce an alternative path to the current due to off state of $S1$ and the current will flow from $S4$ to $D2$.

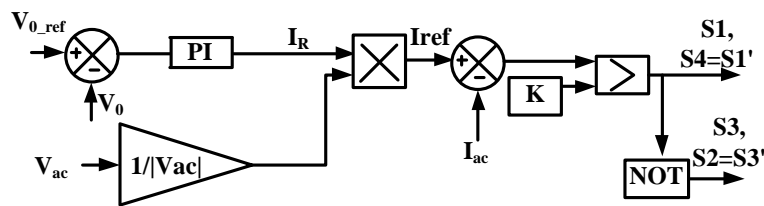


Figure 4. Current control algorithms

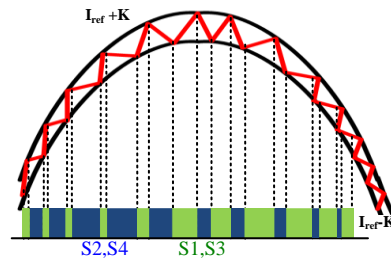


Figure 5. Control pulses for current control

3. CIRCUIT PARAMETER CALCULATION

To derive the expressions, consider the circuit shown in Figure 6, and solve the Kirchoff's current law (KCL) equation in the circuit for the positive half of the cycle of the input voltage as follows.

$$v_{ac} = V_m \sin(\omega t) \tag{1}$$

$$i(t) = i_L(t) + i_C(t) \tag{2}$$

$$i(t) = \frac{1}{L_1} \int v_C(t) dt + i_C(t) \tag{3}$$

where the input voltage is v_{ac} , transformer primary current is $i(t)$, the inductor current is $i_L(t)$ and the current through the capacitor is $i_C(t)$. If KVL is applied across the capacitor, the capacitive voltage is derived by (4).

$$v_C(t) = V_m \sin(\omega t) - nV_0 \tag{4}$$

using from (1) to (4), the primary side current in the inductor is derived as shown in.

$$i(t) = -\frac{1}{L} \left[\frac{V_m}{\omega} \sin(\omega t) + nV_0 t \right] + \omega C.V_m \cos(\omega t) \tag{5}$$

For a very small duration of Δt during which the switch S4 is on, the current can be written as shown in:

$$i(t + \Delta t) = -\frac{1}{L} \left[\frac{V_m}{\omega} \sin(\omega(t + \Delta t)) + nV_0(t + \Delta t) \right] + \omega C.V_m \cos(\omega(t + \Delta t)) \tag{6}$$

the error between (5) and (6), will produce a value which when equal to K will cause S4 to be off.

$$i(t) - i(t + \Delta t) = K \tag{7}$$

Taking the approximation of Δt to be very small the maximum number of turns for the transformer can be derived as follows.

$$n \frac{K * L_1}{V_0 * \Delta t_{max}} \tag{8}$$

The maximum value of K can be calculated by considering the maximum possible voltage across the inductor L and using (8).

$$L \frac{(i(t) - i(t + \Delta t))}{\Delta t} = V_m$$

where K_{max} can be obtained using (8).

$$K \frac{V_m * \Delta t}{L} \tag{9}$$

In (8) and (9), Δt depends on the minimum turn-on time required by the switch and thus would change with the type of switch being used. The maximum value of the primary current $i(t)$ is limited by the current limitation in the windings of the transformer which is I_{rated} . Using this we can calculate the value of the inductance L given by (10).

$$L_1 = \frac{1}{I_{rated}} \left[\frac{1}{\omega} + \omega C \right] * V_m \tag{10}$$

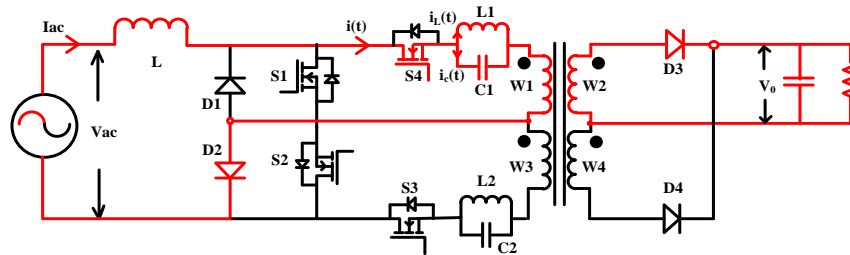


Figure 6. Control algorithms for input power factor and current control

4. SIMULATION RESULTS

Simulation results of the proposed converter are presented in Figures 7-10. Figure 7(a) shows the input voltage and input current, the input voltage is 230 V rms and AC side current is 20.5 A rms. Figure 7(b) shows the magnified view of the current tracking with reference and actual current plots. A comparison of Figure 5 with Figure 7(b) can be done to infer the proper functioning of the proposed algorithm. It is visible from Figure 7(b) that the input AC current remains in the band of I_{ref} and $I_{ref} + k$ as discussed earlier. For the simulation data, the K is chosen to be 0.5.

To check the dynamic performance, a load variation test is done. Figure 8(a) shows the output power and input AC current. The load variation occurs at the instant of 1 sec and 2 sec. The demand in the output power is compensated by the increase in the current. When the load is increased during 1 sec, a change in the current takes place to match the demand causing new value of the current to settle at 28 A. The demanded power is matched beyond this instant but ripple in the output power increases leading to the decrement in the efficiency which is shown by the graph in Figure 8(a). In Figure 8(b), the reference voltage is maintained at

150 V which is tracked by the actual DC link voltage, even after the load disturbances at 1 and 2 sec. The DC link voltage again stabilizes and reaches to 150 V, whereas the load current is increased from 10 A to 15 A, and finally to 30 A. A zoomed view of the transformer primary current T1 and T2 is also shown in Figure 8(c).

Figure 8(d) shows the variation in the output power when the reference voltage is changed thus suggesting the proper functioning of the control method. The change in the reference took place at the instant of 1 sec and 2 sec. The reference voltage is 100 V between 0-1 sec and it increases to 150 V between 1-2 sec, and finally between 2-3 sec it is again changed to 200 V. This shows the capability of the controller to achieve a wide range of the output voltage variations.

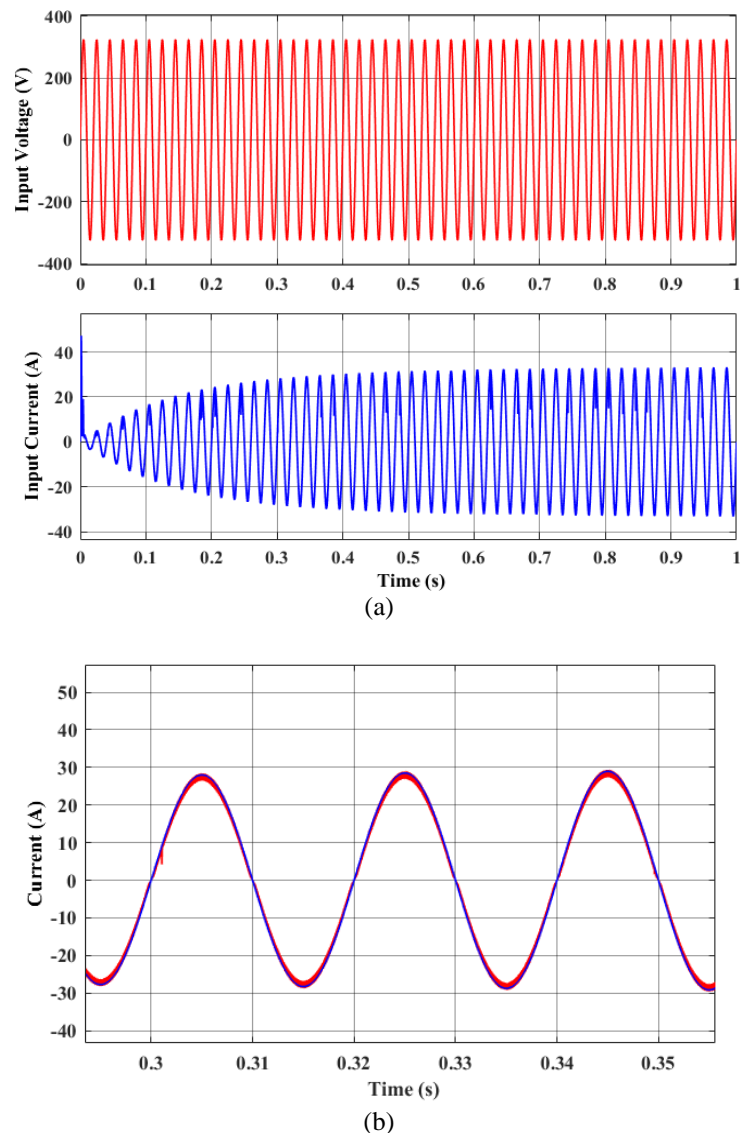


Figure 7. The simulation waveforms for (a) phase voltage and phase current and (b) tracking of the actual current to the reference

The variation in efficiency with respect to turn ratio is shown in Tables 2-4. These tables show the effect of the load voltage and turns ratio on the efficiency. The DC voltage ripple and the current harmonic distortion are the important factors for enhancing the power quality of the converter. The Tables 1-3 also shows the variation in the output voltage ripple and current THD for a given output voltage, keeping the turns ratio constant. Three values of turn ratio of $5/2$, $5/3$, and $25/4$ are considered in the tables. From the data obtained it is suggestible to go with the voltage level of 180 V, 300 V, and 150 V from Tables 2-4, respectively. The circuit parameters that are used for the simulation are also shown in the Table 5.

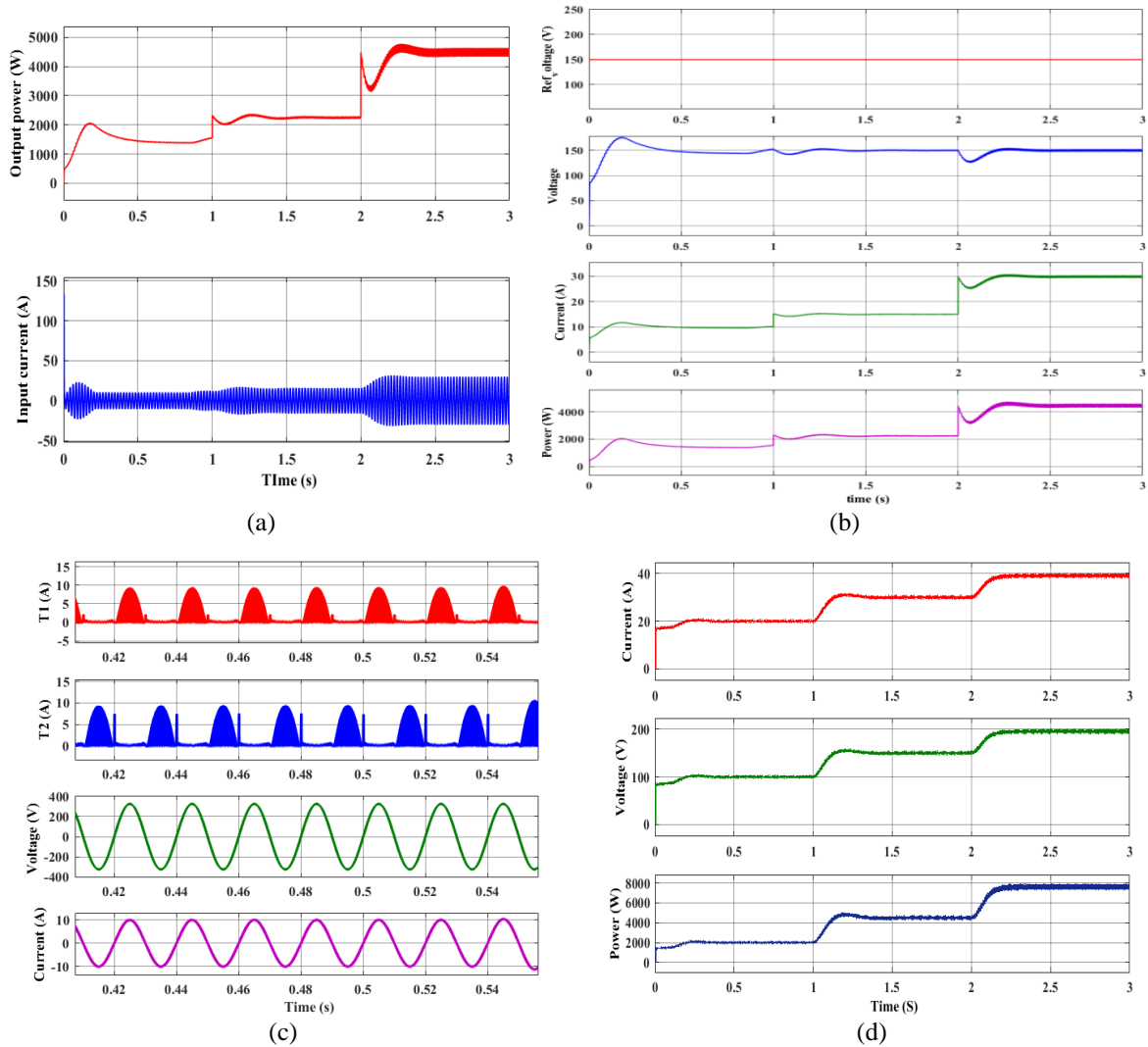


Figure 8. The simulation waveform (a) variation in the output power and the AC current with change in load, (b) output voltage, current and power, (c) its zoomed view, and (d) output voltage, current and power with changing reference voltage

Table 2. For $N_1/N_2=5/2$

V_0	$\Delta V_0/V_0$	THD	$\eta\%$
400	1.5	1.6	91
350	1.5	1.5	92
300	1.5	1.4	94
260	1.5	1.8	93

Table 3. For $N_1/N_2=5/3$

V_0	$\Delta V_0/V_0$	THD	$\eta\%$
400	1.5	1.6	91
350	1.5	1.5	92
300	1.5	1.4	94
260	1.5	1.8	93

Table 4. For $N_1/N_2=25/4$

V_0	$\Delta V_0/V_0$	THD	$\eta\%$
200	2	2.6	92
180	2.5	2.1	94
150	2	1.8	94
100	2	1.5	92

Table 5. Simulation circuit parameters

AC voltage	230 V rms
filter inductance	1 mH
Capacitance	100 μ F
Inductor value	200 μ H
Output capacitor	600 μ F

5. EXPERIMENTAL RESULTS

To conduct the experiment, a 1.0 kW prototype has been designed in the laboratory. Figure 9(a) shows the experimental setup of the proposed converter implemented in the laboratory. The parameters used in the experimental setup are shown in the Table 6 with the values of the output capacitor, inductor and input voltage. The control algorithm has been realized using typhoon 402 field-programmable gate array (FPGA)

based hardware in loop device. The control signals are given to the MOSFET IRFP260N arranged in the configuration of the proposed circuit. The two transformers are having the turn ratio of 5/2. The input side diode is FE30JP which is a back-to-back connected diode. The same FE30JP is used for the output diode connection to a resistive load. The current in the transformer primary of T1 and T2 is shown in the Figure 9(b) with the phase voltage. As simulated earlier in the above section, the positive half of the voltage occurs when the switch T1 is in the conducting mode and the switch T2 is in the conduction mode in the negative half of the cycle of the input voltage. Both of these current waveforms are shown in Figure 9(b) with the stable dc-link voltage of 120 V. The test is performed under the changing load scenario and the associated waveforms are shown in Figure 10. In the Figure 10(a), the DC link voltage is shown for the 10% change in the load. It can be seen that the voltage is constant at 150 V even after change in the current from 5.2 A to 4.7 A peak after disturbance. The power factor correction is visible in Figure 10(b) as the phase of the input voltage (230 V rms) and current remains same. The reference tracking is shown in Figure 10(c). In Figure 10(d), the reference voltage is changed from 150 V to 120 V. In response to this change the control algorithm brings down the DC link voltage to 120 V and finally settles to this value. Further

Table 6. Experimental circuit parameters

S.no	Parameters	rating
1	AC voltage	230 Vrms
2	Input inductor	1 mH
4	Inductor value	200 uH
5	Output capacitor	600 uF

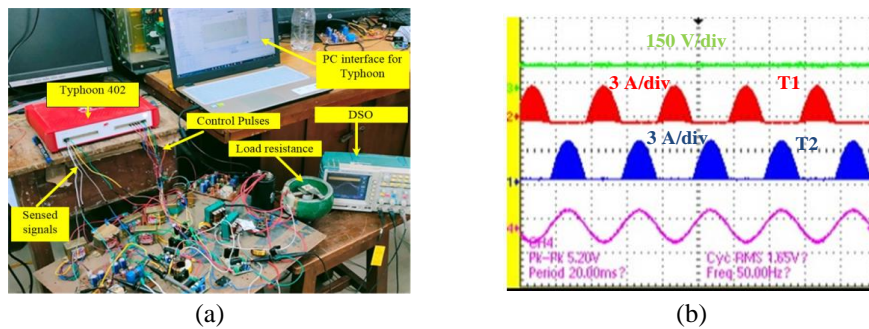


Figure 9. The view and waveforms from the (a) experimental setup and (b) zoomed-in DC link voltage with input AC current and currents in the transformer primary and the secondary side

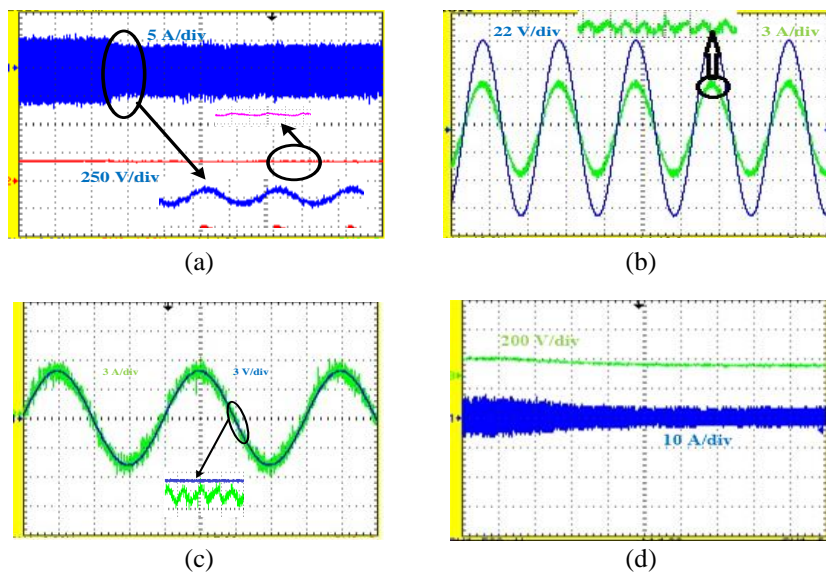


Figure 10. Experimental results showing (a) DC link voltage control and load input current under changing load, (b) in-phase current with respect to voltage showing power factor correction, (c) tracking of reference current and voltage, and (d) response for changing reference voltage

6. CONCLUSION

This paper presents a novel single-stage AC/DC converter that reduces the use of the diode bridge which is required at the input in the majority of the single-stage AC/DC converter. As compared to two-stage AC/DC conversion with power factor correction, in the proposed converter there is no intermediate DC link which reduces the need for a bulky electrolytic capacitor. The proposed converter will find vital use in the high-power DC charging by reducing components and providing high voltage when connected in cascaded connection and higher power when used in a parallel configuration. The converter also provides a wide range of output voltage for a fixed transformer turns ratio. The simulation study is done on MATLAB/Simulink and tested the control method under the scenario of changing load and changing reference. The converter and control performance are verified through the laboratory experimental model using typhoon 402 FPGA based hardware in loop device.




REFERENCES

- [1] R. Kushwaha and B. Singh, "A modified bridgeless cuk converter based EV charger with improved power quality," *2019 IEEE Transportation Electrification Conference and Expo (ITEC)*, 2019, pp. 1-6, doi: 10.1109/ITEC.2019.8790509.
- [2] B. Singh and R. Kushwaha, "EV battery charger with non-inverting output voltage-based bridgeless PFC Cuk converter," *IET Power Electronics*, vol. 12, no. 13, pp. 3359-3368, 2019, doi: 10.1049/iet-pel.2019.0037.
- [3] R. Kushwaha and B. Singh, "A modified luo converter-based electric vehicle battery charger with power quality improvement," in *IEEE Transactions on Transportation Electrification*, vol. 5, no. 4, pp. 1087-1096, Dec. 2019, doi: 10.1109/TTE.2019.2952089.
- [4] B. Singh and R. Kushwaha, "A PFC based EV battery charger using a bridgeless SEPIC converter," *2016 IEEE 7th Power India International Conference 2016*, pp. 1-6, doi: 10.1109/POWERL.2016.8077260.
- [5] R. Kushwaha and B. Singh, "A power quality improved EV charger with bridgeless cuk converter," *2018 IEEE International Conference on Power Electronics, Drives and Energy Systems (PEDES)*, 2018, pp. 1-6, doi: 10.1109/PEDES.2018.8707701.
- [6] Sin-Woo Lee and Hyun-Lark Do, "Efficient bridgeless PFC converter with reduced voltage stress," *International Journal of Circuit Theory and Application*, vol. 44, no. 7, pp. 1455-1467, 2016, doi: 10.1002/cta.2170.
- [7] E. H. Ismail, M. A. Al-Saffar, A. J. Sabzali, and A. A. Zerai, "Single-stage single-switch PFC converter for wide-input extreme step-down voltage applications," *International Journal of Circuit Theory and Applications*, vol. 41, no. 7, pp. 701-720, 2013, doi: 10.1002/cta.813.
- [8] H.-J. Chiu, Y.-K. Lo, T.-P. Lee, C.-C. Chuang, and S.-C. Mou, "A single-stage phase-shifted full-bridge AC/DC converter with variable frequency control," *International Journal of Circuit Theory and Applications*, vol. 38, no. 8, pp. 867-879, 2010, doi: 10.1002/cta.598.
- [9] R. Kushwaha and B. Singh, "Power Factor Improvement in Modified Bridgeless Landsman Converter Fed EV Battery Charger," in *IEEE Transactions on Vehicular Technology*, vol. 68, no. 4, pp. 3325-3336, April 2019, doi: 10.1109/TVT.2019.2897118.
- [10] J. Gupta, R. Kushwaha, B. Singh and V. Khadkikar, "Improved Power Quality Charging System Based on High Step-Down Gain Bridgeless SEPIC APFC for Light Electric Vehicles," in *IEEE Transactions on Industry Applications*, vol. 58, no. 1, pp. 423-434, Jan.-Feb. 2022, doi: 10.1109/TIA.2021.3120028.
- [11] N. Rathore, S. Gangavarapu, A. K. Rathore and D. Fulwani, "Emulation of loss free resistor for single-stage three-phase PFC converter in electric vehicle charging application," in *IEEE Transactions on Transportation Electrification*, vol. 6, no. 1, pp. 334-345, Mar. 2020, doi: 10.1109/TTE.2020.2976878.
- [12] J. Gupta, R. Kushwaha and B. Singh, "Single Stage Switched Inductor SEPIC Based Charging System for LEVs," *2020 IEEE International Conference on Computing, Power and Communication Technologies (GUCON)*, 2020, pp. 124-129, doi: 10.1109/GUCON48875.2020.9231128.
- [13] A. R. Ghanbari, E. Adib, and H. Farzanehfard, "Single-stage single-switch power factor correction converter based on discontinuous capacitor voltage mode buck and flyback converters," *IET Power Electronics*, vol. 6, no. 1, pp. 146-152, 2013, doi: 10.1049/iet-pel.2012.0191.
- [14] Tsai-Fu Wu and Yu-Kai Chen, "Analysis and design of an isolated single-stage converter achieving power-factor correction and fast regulation," in *IEEE Transactions on Industrial Electronics*, vol. 46, no. 4, pp. 759-767, Aug. 1999, doi: 10.1109/41.778230.
- [15] C. Li, Y. Zhang and D. Xu, "Soft-switching single stage isolated AC-DC converter for single-phase high power PFC applications," *2015 9th International Conference on Power Electronics and ECCE Asia (ICPE-ECCE Asia)*, 2015, pp. 1103-1108, doi: 10.1109/ICPE.2015.7167918.
- [16] C. Li, Y. Zhang, Z. Cao, and D. Xu, "Single-phase single-stage isolated ZCS current-fed full-bridge converter for high-power AC/DC applications," in *IEEE Transactions on Power Electronics*, vol. 32, no. 9, pp. 6800-6812, Sep. 2017, doi: 10.1109/TPEL.2016.2623771.
- [17] U. R. Prasanna, A. K. Singh, and K. Rajashekara, "Novel bidirectional single-phase single-stage isolated AC-DC converter with PFC for charging of electric vehicles," in *IEEE Transactions on Transportation Electrification*, vol. 3, no. 3, pp. 536-544, Sep. 2017, doi: 10.1109/TTE.2017.2691327.
- [18] P. Nayak, S. K. Pramanick, and K. Rajashekara, "Isolated single stage AC-DC converter topologies with regenerative snubber circuit for EV application," *IECON 2018-44th Annual Conference of the IEEE Industrial Electronics Society*, 2018, pp. 1285-1290, doi: 10.1109/IECON.2018.8591834.
- [19] U. Nagabalan N. M. J. Swaroopan, "An improved single stage phase shifted control based AC-DC PFC converter for wireless applications," *Wireless Personal Communications*, vol. 117, no. 4, pp. 2853-2864, 2021, doi: 10.1007/s11277-020-07051-5.
- [20] W.-Y. Choi and M.-K. Yang, "High-efficiency isolated SEPIC converter with reduced conduction losses for LED displays," *International Journal of Electronics*, vol. 101, no. 11, pp. 1495-1502, 2014, doi: 10.1080/00207217.2013.874044.
- [21] B. Zhang, S. Xie, J. Xu, K. Xu, and Z. Li, "An optimized single-stage isolated phase-shifted full-bridge based Swiss-rectifier," *IECON 2019-45th Annual Conference of the IEEE Industrial Electronics Society*, 2019, pp. 6581-6586, doi: 10.1109/IECON.2019.8926934.
- [22] S. Jeong, J. Kwon, and B. Kwon, "High-efficiency bridgeless single-power-conversion battery charger for light electric vehicles," in *IEEE Transactions on Industrial Electronics*, vol. 66, no. 1, pp. 215-222, Jan. 2019, doi: 10.1109/TIE.2018.2826458.




- [23] H. Belkamel, K. Hyungjin, K. Beywongwoo, Y. Shin, and S. Choi, "Bi-directional single-stage interleaved totem-pole AC-DC converter with high frequency isolation for on-board EV charger," *2018 IEEE Energy Conversion Congress and Exposition (ECCE)*, 2018, pp. 6721-6724, doi: 10.1109/ECCE.2018.8557933.
- [24] K. Kim, J. Kwon, and B. Kwon, "Single-switch single power-conversion PFC converter using regenerative snubber," in *IEEE Transactions on Industrial Electronics*, vol. 65, no. 7, pp. 5436-5444, July 2018, doi: 10.1109/TIE.2017.2774765.
- [25] M. Z. Efendi, F. D. Murdianto, F. A. Fitri, and L. Badriyah, "Power factor improvement on LED lamp driver using BIFRED converter," *TELKOMNIKA (Telecommunication Computing Electronics and Control)*, vol. 18, no. 1, pp. 571-578, Feb. 2020, doi: 10.12928/TELKOMNIKA.v18i1.13160.
- [26] P. Nayak and K. Rajashekara, "Single-stage Bi-directional matrix converter with regenerative flyback clamp circuit for EV battery charging," *2019 IEEE Transportation Electrification Conference and Expo (ITEC)*, Jun. 2019, pp. 1-6, doi: 10.1109/ITEC.2019.8790462.
- [27] S. Ojha, and A. K. Pandey, "Close loop V/F control of voltage source inverter using sinusoidal PWM, third harmonic injection PWM and space vector PWM method for induction motor," *International Journal of Power Electronics and Drive Systems (IJPEDS)*, vol. 7, no. 1, pp. 217-224, Mar. 2016, doi: 10.11591/ijpeds.v7.i1.pp217-224.

BIOGRAPHIES OF AUTHORS



Anurag Sharma    received the Bachelor of Technology in Electrical and Electronics Engineering in 2013 from United College of Engineering and Research, Prayagraj, Uttar Pradesh, India. Master of Technology in Power Electronics and Drives in 2017 from Motilal Nehru National Institute of Technology Allahabad, Prayagraj, Uttar Pradesh, India. He is presently pursuing Ph.D from Motilal Nehru National Institute of Technology Allahabad, Prayagraj, Uttar Pradesh, India. He can be contacted at email: anuragsharma@mnnit.ac.in.



Dr. Rajesh Gupta    received the Bachelor of Technology in 1993 from Madan Mohan Malaviya Engineering College, Gorakhpur, Uttar Pradesh, India. Master of Technology in 1995 from Birla Institute of Technology, Ranchi, India. Ph.D in 2007 from Indian Institute of Technology Kanpur, Uttar Pradesh, India. He is presently a Professor and Head of Department of Electrical Engineering, Motilal Nehru National Institute of Technology Allahabad, Prayagraj, Uttar Pradesh, India. His research interests include power conversion of renewable energy resources, power electronics converters and its control, digital controllers, and electric vehicles. He guided 12-Ph.D and 50 masters students. He has filed patents in the area of bidirectional and hybrid converters. He published around 125 papers in reputed International Journals and Conferences. He is a recipient of 2013 IEEE Outstanding Branch Counsellor Award of Region-10 of IEEE. He is also recipient of 2014 IEEE Outstanding Volunteer Award of IEEE Uttar Pradesh Section. He was a first prize winner of VI mantra contest in 2006, organized by National Instruments. Two of his Ph.D students and two masters students have won POSOCO awards sponsored by Power Grid Corporation of India, in association with IIT Delhi. His name appeared in top 2% scientists in the world under the category of "Electrical & Electronics", published by Stanford University consecutively for the years 2020 and 2021. Dr. Gupta is serving as Associate Editor of IEEE Transactions on Energy Conversion, and IEEE Power and Energy Society Letters. He can be contacted at email: rajeshgupta@mnnit.ac.in.